# DYNAMIC MODEL OF A SELF-EXCITED INDUCTION GENERATOR WITH FUNDAMENTAL STRAY LOAD AND IRON LOSSES

by

## *Mateo BAŠIĆ\*, Dinko VUKADINOVIĆ, and Ivan GRGIĆ*

Faculty of Electrical Engineering, Mechanical Engineering and Naval Architecture,
University of Split, Split, Croatia

*This paper considers a dynamic model of a self-excited induction generator that takes into account the fundamental stray load and iron losses. The model is described with the same number of differential equations as the conventional induction machine model. Determination of the stray load and iron losses resistances does not involve any tests other than those imposed by the international standards nor does it require any details about induction machine materials or geometry. The dynamic analysis has been carried out for the case of a wind turbine-driven self-excited induction generator. The steady-state analysis, on the other hand, has been carried out for the case of a load-independent prime mover. The considered advanced model, aside from being compared with the conventional model, has been experimentally validated for two different-efficiency induction machines, both rated 1.5 kW.*

Key words: *equivalent circuits, induction machines, iron losses, stray load losses,
renewable energy, wind turbines*

## Introduction

During the last decades, the substantial rise in energy demand has resulted in growing production and use of fossil fuels for power generation. However, this raised many environmental concerns so, consequently, renewable energy sources have been receiving increasing attention. In this context, wind energy conversion systems (WECS) have emerged as one of the most promising alternatives to conventional power generation systems [1]. In remote, small-power WECS, self-excited induction generators (SEIG) are often recognized as a low-cost alternative to permanent-magnet synchronous generators. This is due to their simple and rugged construction, low maintenance, small size and inherent protection against overloads and short-circuits. However, in off-grid operation, the SEIG requires external capacitors for excitation. In addition, both the magnitude and frequency of its terminal voltage significantly vary with the applied load and the speed of the prime mover. To compensate for this variation, various control schemes have been proposed [2-4], but this subject is out of the scope of this research.

The iron losses and the stray load losses (SLL) represent the two loss components that are most often neglected in induction machine (IM) models. Both these losses are identifiable from the tests imposed by the international standards IEEE 112-B [5] and IEC 60034-2-1 [6]. Habitually, about 1-4% of the IM rated power is assigned to the iron losses, whereas 0.5-3% of

---

the IM rated power is assigned to the SLL at full load [7]. The negative impact of the iron losses and the SLL – as well as of any other type of losses – on the IM's efficiency, loading capacity, operating temperature, and expected lifetime is self-evident. In addition, their negative impact on the IM vector control in terms of misalignment of the reference vector was reported in [4, 8, 9], so the importance of their assessment is not to be underestimated.

The iron losses are standardly modeled in IM equivalent circuits by means of the equivalent resistance, $R_m$, placed in parallel with the main inductance, $L_m$ [8-10]. However, in this way the number of the first-order differential equations describing the IM is increased by two compared to the conventional model. This problem can be circumvented by shifting the iron-loss resistance in front of the stator leakage inductance, as first proposed by Shinnaka in [11]. The Shinnaka configuration was later considered and experimentally verified in [4, 12, 13].

In those very few papers that consider the SLL as part of the IM equivalent circuit, the corresponding equivalent resistance is usually placed in parallel with the stator and/or rotor leakage inductance [8, 14], thus additionally increasing the order of the IM model. An alternative SLL configuration in which the stray-loss resistance is placed in series with the stator phase resistance was proposed by Chang in [15]. The Chang configuration was also considered in [10] where its validity was proven experimentally. However, in this configuration, the iron-loss resistance is placed in parallel with the main inductance, so the previously mentioned problem, *i.e.*, the increase of the IM model's order, is still present.

In [16], the hybrid Shinnaka-Chang configuration was for the first time proposed for modeling of the IM iron losses and SLL. The model's validity was checked for the case of the unregulated SEIG. Dynamic performance was assessed for the case of a load-dependent prime mover, *i. e.*, wind turbine (WT), whereas steady-state operation was assessed for the case of a load-independent prime mover in wide ranges of load and rotor speed. Here, the analysis is extended by addition of the simulation and experimental results obtained for the stator current and also by addition of the simulation results obtained for the SEIG loss distribution.

## Modeling of a wind energy conversion system

The basic configuration of the considered WECS is shown in fig. 1. The WECS consists of a WT coupled to an SEIG via a gearbox, a capacitor bank, and a resistive load, which is applied by closing the switch *S*. The fact that the considered WECS is lacking any means of controlling the SEIG terminal voltage is not relevant here because its main purpose is to serve as a means of verification of the proposed IM model.

### Proposed SEIG model

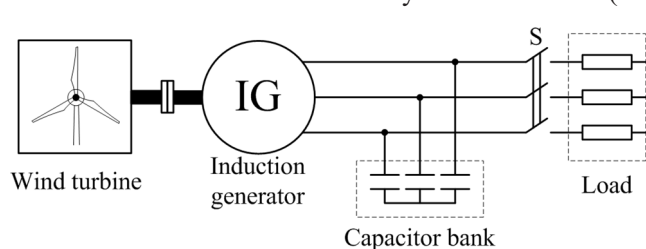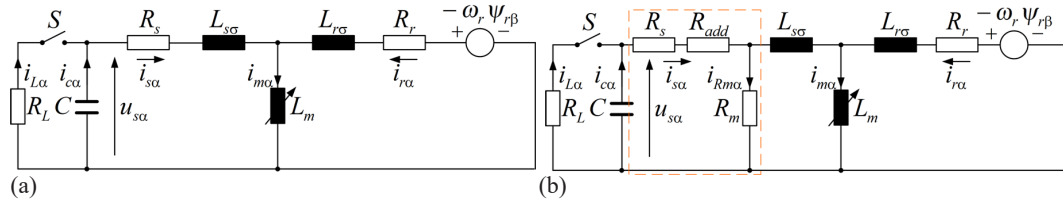Figure 2 shows the equivalent circuits of both the conventional and the proposed dynamic SEIG model in the stationary reference frame (only *α*-axis). The proposed SEIG model takes into account both the iron and stray losses by means of the corresponding equivalent resistances – $R_m$ and $R_{add}$, respectively. The configuration of the proposed equivalent circuit in fact corresponds to a hybrid *Shinnaka-Chang* configuration, as discussed before.



**Figure 1. Basic WECS configuration**

Bašić, M., *et al.*: Dynamic Model of a Self-Excited Induction Generator ...
THERMAL SCIENCE: Year 2018, Vol. 22, Suppl. 3, pp. S797-S807

S799

**Figure 2. Single-phase SEIG equivalent circuits in the stationary reference frame (α-axis):**
**(a) conventional model and (b) proposed model**

The differential equations describing the conventional dynamic SEIG model are given:

$$-u_{s\alpha} = R_s i_{s\alpha} + \frac{\mathrm{d}\psi_{s\alpha}}{\mathrm{d}t}, \qquad -u_{s\beta} = R_s i_{s\beta} + \frac{\mathrm{d}\psi_{s\beta}}{\mathrm{d}t} \tag{1}$$

$$0 = R_r i_{r\alpha} + \frac{\mathrm{d}\psi_{r\alpha}}{\mathrm{d}t} + \omega_r \psi_{r\beta}, \qquad 0 = R_r i_{r\beta} + \frac{\mathrm{d}\psi_{r\beta}}{\mathrm{d}t} - \omega_r \psi_{r\alpha} \tag{2}$$

$$\psi_{s\alpha} = L_{s\sigma} i_{s\alpha} + L_m i_{m\alpha}, \qquad \psi_{s\beta} = L_{s\sigma} i_{s\beta} + L_m i_{m\beta} \tag{3}$$

$$\psi_{r\alpha} = L_{r\sigma} i_{r\alpha} + L_m i_{m\alpha}, \qquad \psi_{r\beta} = L_{r\sigma} i_{r\beta} + L_m i_{m\beta} \tag{4}$$

$$i_{m\alpha} = i_{s\alpha} + i_{r\alpha}, \qquad i_{m\beta} = i_{s\beta} + i_{r\beta} \tag{5}$$

$$T_e = \frac{3}{2} p \frac{L_m}{L_r} (\psi_{r\alpha} i_{s\beta} - \psi_{r\beta} i_{s\alpha}) = T_m - J \frac{\mathrm{d}\omega_r}{\mathrm{d}t} - B\omega_r \tag{6}$$

$$u_{c\alpha} = u_{s\alpha} = \frac{1}{C} \int_0^t i_{c\alpha} \mathrm{d}t + u_{s\alpha o}, \qquad u_{c\beta} = u_{s\beta} = \frac{1}{C} \int_0^t i_{c\beta} \mathrm{d}t + u_{s\beta o} \tag{7}$$

$$u_{L\alpha} = u_{s\alpha} = R_L i_{L\alpha}, \qquad u_{L\beta} = u_{s\beta} = R_L i_{L\beta} \tag{8}$$

$$i_{s\alpha} = i_{L\alpha} + i_{c\alpha}, \qquad i_{s\beta} = i_{L\beta} + i_{c\beta} \tag{9}$$

The Thevenin equations for the elements in the dashed rectangle in fig. 2(b) are defined:

$$R_{sT} = \frac{(R_s + R_{add}) R_m}{R_s + R_{add} + R_m} \tag{10}$$

$$u_{sT\alpha} = u_{s\alpha} \frac{R_m}{R_s + R_{add} + R_m}, \qquad u_{sT\beta} = u_{s\beta} \frac{R_m}{R_s + R_{add} + R_m} \tag{11}$$

$$i_{sT\alpha} = i_{s\alpha} \frac{R_s + R_{add} + R_m}{R_m} - \frac{u_{s\alpha}}{R_m}, \qquad i_{sT\beta} = i_{s\beta} \frac{R_s + R_{add} + R_m}{R_m} - \frac{u_{s\beta}}{R_m} \tag{12}$$

Hence, the differential equations describing the proposed dynamic SEIG model are obtained by taking into account eqs. (1)-(12) and by simply introducing the substitutions $R_s \rightarrow R_{sT}$, $u_{s\alpha} \rightarrow u_{sT\alpha}$, $u_{s\beta} \rightarrow u_{sT\beta}$, $i_{s\alpha} \rightarrow i_{sT\alpha}$, and $i_{s\beta} \rightarrow i_{sT\beta}$ in eqs. (1)-(6). Thus, the resulting model is of the same order as the conventional model.

### Determination of IM model parameters

In this research, two squirrel-cage IM (4-pole, star-connected, rated 1.5 kW) with die-cast aluminum rotor are considered: one of the efficiency class IE1 (in the following: *IM*1) and the other of the efficiency class IE3 (in the following: *IM*2), according to IEC 60034-30-1 [17].

The magnetic saturation, being essential for the operation of the SEIG, is accounted for by representing the main inductance, $L_m$, as variable with respect to the magnetizing current, $I_m$. This variation is determined from the no-load test.
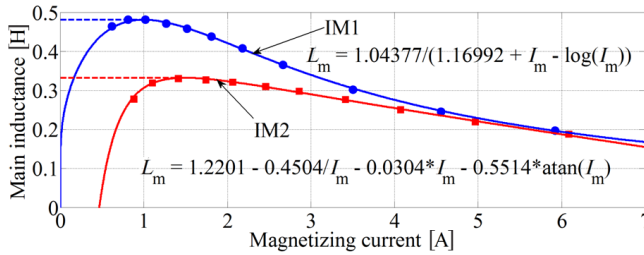


**Figure 3. Measured magnetizing characteristics approximated by curves**

Figure 3 shows the measured magnetizing characteristics obtained for the two considered IM, along with the corresponding approximation curves. Since the main inductance is rather difficult to determine with high accuracy for low values of the magnetizing current, it is within this unsaturated region approximated by a constant value (depicted by the dashed lines in fig. 3). By this, the validity of the model is to some extent sacrificed for simplicity and numerical stability. On the other hand, steady-state operating points of any SEIG are always located in the saturated region.
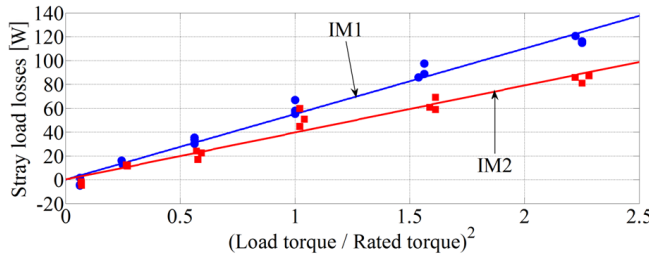


**Figure 4. Corrected stray load losses vs. torque squared**

In order to determine the SLL, the standards IEEE 112-B and IEC 60034-2-1 require performing thermal test at the rated load, no-load test, and variable-load test at rated thermal conditions [5, 6]. Here, the measurements were repeated three times for each load torque value, whereas high measurement accuracy was ensured by utilizing the power analyzer Norma 4000 (Fluke) and the torque transducer TMB 308 (Magtrol). Figure 4 shows the corrected SLLs versus the load torque squared characteristics determined for the two considered IM [5, 6].

The $R_{add}$ value is derived from the no-load and variable-load test data. With the full theoretical background provided in [10], only the final expression is here given:

$$R_{add} = \frac{(P_e - 3R_s I_s^2 - P_{Fe,conv})(1-s) - P_m - P_{loss,mech}}{3(I_s^2 - (1-s)I_{s,0}^2)} \tag{13}$$

In the proposed model, fig. 2(b), the stray-loss resistance takes its share of the total no-load losses, so the actual iron losses, $P_{Fe}$, are determined by subtracting the stray no-load losses from the conventional iron losses [10] (the stator phase resistance ratio in eq. (14) provides a quick temperature correction of the stray-loss resistance):

$$P_{Fe} = P_{Fe,conv} - 3I_{s,0}^2 \frac{R_{s,no-load}}{R_{s,load}} R_{add} \tag{14}$$

Bašić, M., *et al.*: Dynamic Model of a Self-Excited Induction Generator ...
THERMAL SCIENCE: Year 2018, Vol. 22, Suppl. 3, pp. S797-S807

S801

Once the actual iron losses are known, the corresponding $R_m$ value can be determined as [12]:

$$R_m = \frac{Q_0^2 + P_{Fe}^2}{3I_{s,0}^2 P_{Fe}}$$ (15)

Figure 5 shows the conventional and actual iron losses versus the stator flux linkage magnitude (in the following: *stator flux*). In both IM, the conventional iron losses at rated stator flux are of about the same value as the SLL at rated torque. The $R_m$ value was calculated from eq. (15) for the values of $Q_0$, $P_{Fe}$, and $I_{s,0}$ that correspond to the rated stator flux (the ellipse in fig. 5).
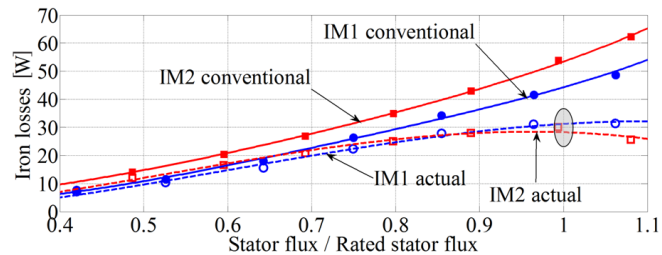


**Figure 5. Conventional and actual iron losses *vs.* stator flux**

*Wind turbine model*

Wind turbines convert the kinetic energy of the wind into mechanical energy handed over to an electric generator shaft. The ratio between the WT mechanical power, $P_{WT}$, and the wind power, $P_w$, is defined as the power coefficient, $C_p$. This coefficient depends on the blade pitch angle and the tip speed ratio, $\lambda$, which is in turn defined:

$$\lambda = \frac{\omega_{WT} R}{v_w}$$ (16)

Small WT, as is the one considered in this paper, usually have constant pitch angle, which leaves $C_p$ depending solely on $\lambda$. By taking this into account, the power coefficient can be approximated by the following generic equation [18-20]:

$$C_p(\lambda) = c_1 \left( \frac{c_2}{\lambda_i} - c_3 \right) e^{-c_4/\lambda_i} + c_5 \lambda$$ (17)

where

$$\lambda_i = 1/(1 - 0.035\lambda)$$ (18)

The coefficients $c_1$ to $c_5$ depend on the aerodynamics of the blades and $c_1 = 0.294$, $c_2 = 85$, $c_3 = 5.3$, $c_4 = 14.5$, and $c_5 = 0.00068$ were assigned, respectively. The guiding principle for selecting these values was to obtain a typical small WT that is suitable for the analyzed IM. This yielded a WT of the following rated values: $P_t = 1.5$ kW, $v_w = 11$ m/s, $\omega_{WT} = 44$ rad/s, and $R = 1.5$ m ($\lambda = 6$).

The mechanical torque produced by the WT is given by:

$$T_{WT} = \frac{1}{2} \rho R^3 \pi v_w^2 \frac{C_p(\lambda)}{\lambda}$$ (19)

Note that in the considered WECS (fig. 1), the WT rotor is not coupled directly to the generator. A gearbox is inserted to adapt the WT to the SEIG so the mechanical torque and the rotor speed delivered to the SEIG shaft at the rated wind speed conditions closely correspond to the rated torque and speed values of the used IM (*i. e.*,
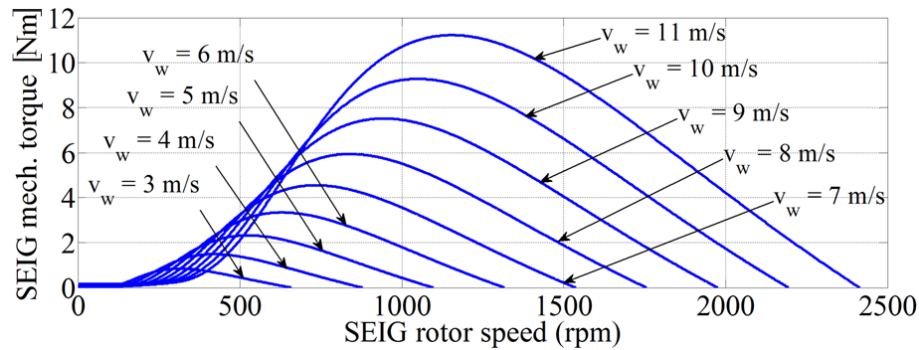
S802

Bašić, M., *et al.*: Dynamic Model of a Self-Excited Induction Generator ...
THERMAL SCIENCE: Year 2018, Vol. 22, Suppl. 3, pp. S797-S807

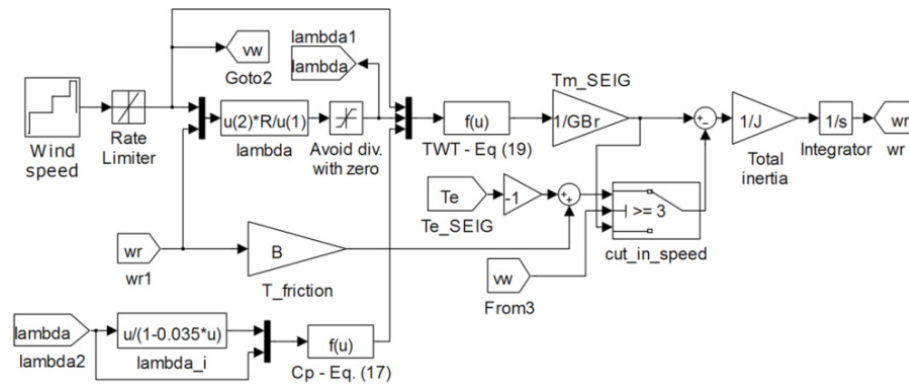**Figure 6. The SEIG mechanical torque *vs.* rotor speed**



**Figure 7. The WT model in MATLAB/Simulink**

about 10 Nm and 1400 rpm, respectively). The resulting characteristics of the SEIG mechanical torque versus the SEIG rotor speed were obtained as in fig. 6.
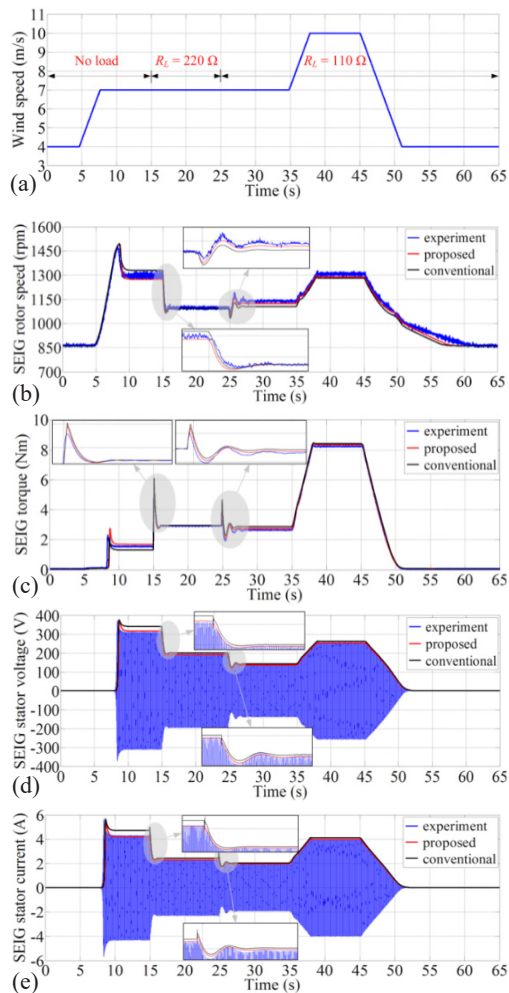
## Results and discussion

The simulation model of the WECS was built in the MATLAB/Simulink. The proposed SEIG model was built based on the respective differential equations, whereas the conventional SEIG model is then obtained by setting $R_{add}$ to zero and $R_m$ to infinity (*i. e.*, to a very large value, for practical reasons). The simulation model of the WT including the gearbox is shown in fig. 7 (*GBr* denotes the gearbox ratio). The WT emulator was developed as part of the WECS experimental setup by using a separately-excited speed-controlled DC motor. The corresponding emulation algorithm was executed by using the DS1104 controller board; the IM's mechanical torque was measured by means of the torque transducer TMB 308.

### *Dynamic performance analysis*

Figures 8 and 9 show the time responses of the selected WECS's variables to changes in wind speed and load, recorded for the two IM. The excitation capacitance was set to 50 μF per phase, whereas two distinct values of the load resistance were used, namely 220 Ω and 110 Ω per phase.

The observation starts at the wind speed of 4 m/s. The corresponding rotor speed is evidently insufficient to initiate the voltage buildup given the used capacitors, so the buildup process
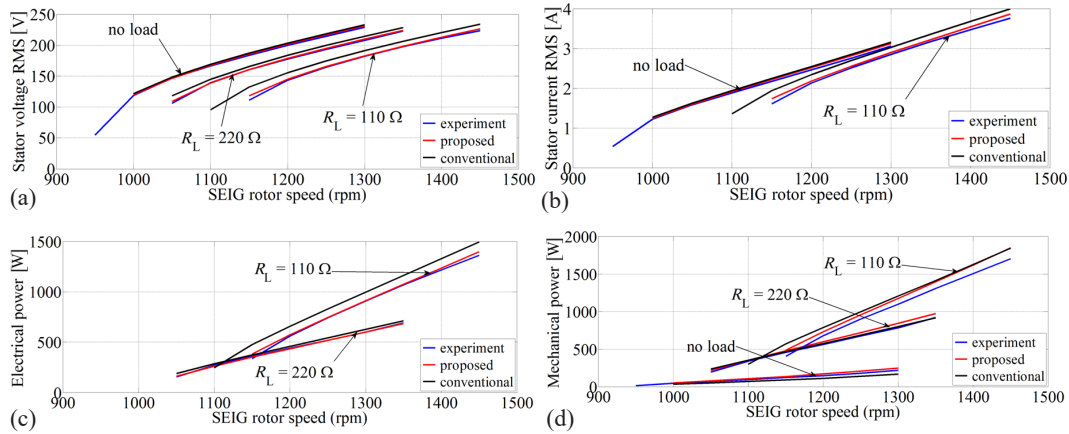
Bašić, M., *et al.*: Dynamic Model of a Self-Excited Induction Generator ...
THERMAL SCIENCE: Year 2018, Vol. 22, Suppl. 3, pp. S797-S807

S803

**Figure 8. The WECS responses to changes in wind speed and load (IM1): (a) wind speed, (b) SEIG rotor speed, (c) SEIG mechanical torque, (d) SEIG stator voltage, and (e) SEIG stator current**
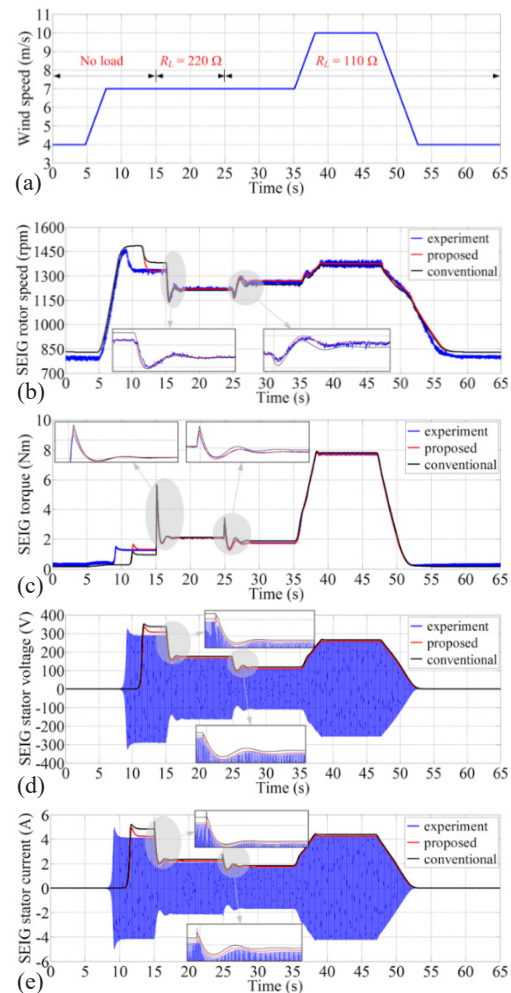
**Figure 9. The WECS responses to changes in wind speed and load (IM2): (a) wind speed, (b) SEIG rotor speed, (c) SEIG mechanical torque, and (d) SEIG stator voltage, and (e) SEIG stator current**

was initiated only after the ramp increase in wind speed, and consequently in the rotor speed, starting at $t = 5$ second. The WECS variables settled at new steady-state values after a short transient period of magnetization. These transients are not subject to consideration here since their analysis would require accurate knowledge of the residual flux in the IM rotor and the initial voltage across the capacitors. The application of load at $t = 15$ second resulted in the voltage drop of about 40%. However, this was still enough to allow an increase in the torque and, consequently, a decrease in the rotor speed (as per fig. 6). The transient period preceding this new steady state is characterized by quickly damped oscillations. The same is valid for the transient period following the application of a more severe load at $t = 25$ second. This time the voltage dropped by another 30% (this is the approximate value), thus approaching the point of demagnetization. As a consequence, the SEIG torque was reduced and the rotor speed increased. Another ramp increase in the wind speed

S804

Bašić, M., *et al.*: Dynamic Model of a Self-Excited Induction Generator ...
THERMAL SCIENCE: Year 2018, Vol. 22, Suppl. 3, pp. S797-S807



**Figure 10. The SEIG steady-state characteristics (IM1): (a) stator phase voltage RMS value, (b) stator phase current RMS value, (c) electrical output power, and (d) mechanical input power**
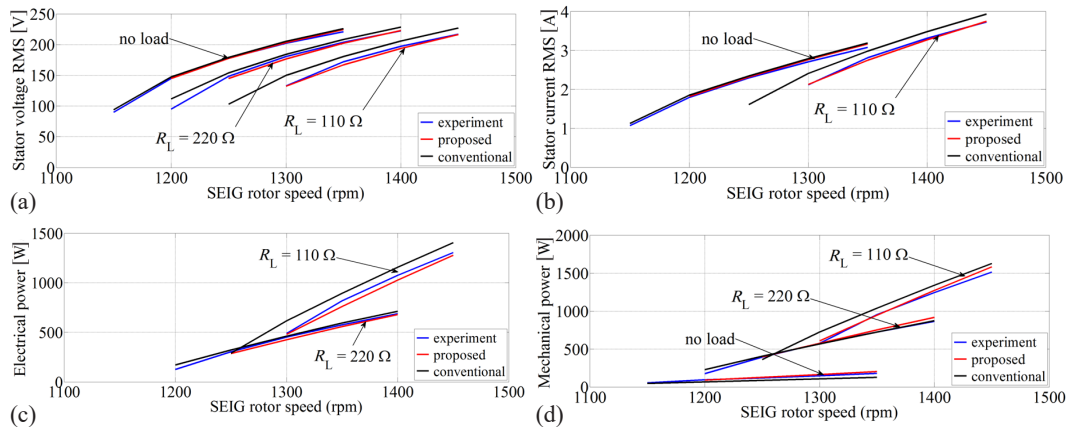


**Figure 11. The SEIG steady-state characteristics (IM2): (a) stator phase voltage RMS value, (b) stator phase current RMS value, (c) electrical output power, and (d) mechanical input power**

occurred at $t$ = 35 s, followed by an increase in all the observed variables. Finally, as the wind speed started to drop to 4 m/s, both of the IM started to demagnetize.
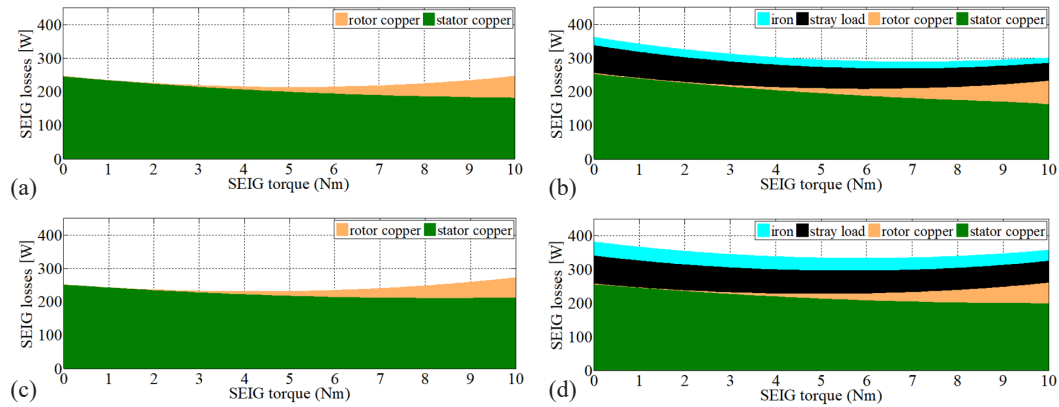
By comparing the simulation and experimental responses it is evident that the proposed WECS model better describes the actual system than the conventional model does. This assertion is valid not only for steady-state operation but for transient periods as well, and for both considered IM.

*Steady-state performance analysis*

Figures 10 and 11 show the steady-state characteristics of the selected SEIG variables, whereas figs. 12 and 13 show distribution of the SEIG losses as a function of the load torque. In this case, a prime mover with the load-independent speed was utilized.

The maximum speed used for each of the load settings in figs. 10 and 11 approximately corresponds to the rated IM voltage (230 V), whereas the minimum speed is the one at which the SEIG is on the verge of demagnetization. Note also that under no load condition, the output power is zero.

Bašić, M., *et al*.: Dynamic Model of a Self-Excited Induction Generator ...
THERMAL SCIENCE: Year 2018, Vol. 22, Suppl. 3, pp. S797-S807

S805

**Figure 12. The SEIG loss distribution (IM1): (a) conventional model, *n* = 1000 rpm, (b) proposed model, *n* = 1000 rpm, (c) conventional model, *n* = 1300 rpm, and (d) proposed model, *n* = 1300 rpm**
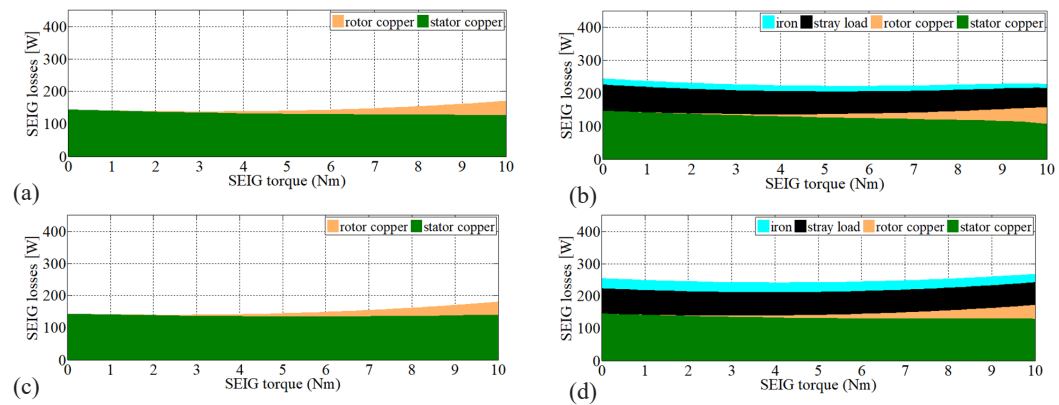


**Figure 13. The SEIG loss distribution (IM2): (a) conventional model, *n* = 1000 rpm, (b) proposed model, *n* = 1000 rpm, (c) conventional model, *n* = 1300 rpm, and (d) proposed model, *n* = 1300 rpm**

The comparison of the simulation and experimental characteristics confirms the superiority of the proposed model for both considered IM. Moreover, the errors introduced by the conventional model seem to increase with load, whereas the proposed model provides fairly accurate assessment of the actual characteristics regardless of the applied load. The only notable differences with respect to the two IMs used concern the achieved speed range and efficiency. Namely, IM2 exhibits somewhat narrower speed range compared to IM1, but on the other hand it expectedly exhibits somewhat higher efficiency.

Higher efficiency class of an IM implies lower total losses, which is confirmed by the results presented in figs. 12 and 13. The rotor copper losses evidently increase with the load torque (*i. e.*, slip), whereas the stator copper losses slightly decrease due to a decrease in the generated stator current. For the same reason, the SLL, seemingly paradoxically, slightly decrease with the increase in load. The iron losses practically do not change with the load, but they increase notably with the rotor speed (*i. e.*, stator frequency). Finally, using the conventional SEIG model inevitably leads to underestimation of the total SEIG losses – in some cases by as much as 130 W.

S806

Bašić, M., *et al.*: Dynamic Model of a Self-Excited Induction Generator ...
THERMAL SCIENCE: Year 2018, Vol. 22, Suppl. 3, pp. S797-S807

## Conclusions

The advanced dynamic model of the SEIG that is considered in this paper takes into account the fundamental iron losses and SLL without increasing the model's order – as compared to the conventional IM model. The respective equivalent resistances are assumed constant, with their values being easily obtained from the tests imposed by international standards. Moreover, no knowledge of the IM materials or geometry is required in the process.

By neglecting the iron losses and/or the SLL in the IM model, considerable errors may be induced in the assessment of the actual SEIG performance. This was proven to be true – based on the comparison of the simulation and experimental results obtained for generated voltage, power, torque, *etc*. – not only for the standard-efficiency IM, but for the premium-efficiency IM as well. For example, it turned out that the conventional SEIG model may underestimate the total IM losses, as compared to the proposed model, by as much as 8.7% (IM1) and 7.5% (IM2) of the IM's rated power.

The proposed model is recognized as suitable for the development of vector control algorithms since such algorithms are all in essence based on the fundamental harmonic component of IM variables, but this is the subject of future research.

## Acknowledgment

## Nomenclature

*Self-excited induction generator*

$B$ – rotational friction coefficient, [kgm$^2$s$^{-1}$]
$C$ – excitation capacitance, [F]
$i_c$ – capacitor current, [A]
$i_L$ – load current, [A]
$i_m$ – magnetizing current, [A]
$i_r$ – rotor phase current, [A]
$i_{Rm}$ – iron loss current, [A]
$i_s$ – stator phase current, [A]
$I_s$ – RMS value of the stator current, [A]
$I_{s,0}$ – RMS value of the stator current from no-load test, [A]
$J$ – moment of inertia, [kgm$^2$]
$L_m$ – magnetizing inductance, [H]
$L_r$ – rotor inductance, [H]
$L_{s\sigma}$ – stator leakage inductance, [H]
$L_{r\sigma}$ – rotor leakage inductance, [H]
$p$ – number of pole pairs, [–]
$P_e$ – electrical input power, [W]
$P_{Fe}$ – actual iron losses, [W]
$P_{Fe,conv}$ – conventional iron losses (accounting for the variation with load as imposed by IEC 60034-2-1), [W]
$P_{loss,mech}$ – friction and windage losses, [W]
$P_m$ – mechanical output power (corrected as imposed by IEEE 112-B), [W]
$Q_0$ – no-load reactive power, [Var]
$R_{add}$ – stray load loss resistance, [Ω]
$R_L$ – load resistance, [Ω]
$R_m$ – iron loss resistance, [Ω]

$R_r$ – rotor phase resistance, [Ω]
$R_s$ – stator phase resistance, [Ω]
$R_{s,load}$ – stator phase resistance value at rated-load thermal conditions, [Ω]
$R_{s,no-load}$ – stator phase resistance value at no-load thermal conditions [Ω]
$s$ – slip, [–]
$T_e$ – electromagnetic torque, [Nm]
$T_m$ – mechanical torque, [Nm]
$u_c$ – capacitor voltage, [V]
$u_L$ – load voltage, [V]
$u_s$ – stator phase voltage, [V]
$\psi_r$ – rotor flux linkage, [Wb]
$\omega_r$ – rotor angular speed, [rads$^{-1}$]

*Wind turbine*

$C_p$ – power coefficient, [–]
$P_t$ – rated power, [W]
$P_w$ – wind power, [W]
$P_{WT}$ – mechanical power, [W]
$R$ – mechanical torque, [Nm]
$v_w$ – wind speed, [ms$^{-1}$]
$\lambda$ – tip speed ratio [–]
$\rho$ – air density [kgm$^{-3}$] (here assumed equal to 1.225 kg/m$^3$)
$\omega_{WT}$ – angular speed [rads$^{-1}$]

*Subscripts*

T – Thevenin equivalents
α – stationary reference frame axe
β – stationary reference frame axe

Bašić, M., *et al.*: Dynamic Model of a Self-Excited Induction Generator ...
THERMAL SCIENCE: Year 2018, Vol. 22, Suppl. 3, pp. S797-S807

S807

## References

[1] Dumnić, B. P., *et al.*, Speed-Sensorless Control Strategy for Multi-Phase Induction Generator in Wind Energy Conversion Systems, *Thermal Science*, *20* (2016), Suppl. 2, pp. S481-S493
[2] Thomsen, B., *et al.*, Faroe Islands Wind-Powered Space Heating Microgrid Using Self-Excited 220-kW Induction Generator, *IEEE Transactions on Sustainable Energy*, *5* (2014), 4, pp. 1361-1366
[3] Margato, E., *et al.*, A New Control Strategy with Saturation Effect Compensation for an Autonomous Induction Generator Driven by Wide Speed Range Turbines, *Energy Conversion and Management*, *5* (2011), 2, pp. 2142-2152
[4] Bašić, M., Vukadinović, D., Vector Control System of a Self-Excited Induction Generator Including Iron Losses and Magnetic Saturation, *Control Engineering Practice*, *21* (2013), 4, pp. 395-406
[5] ***, IEEE Standard Test Procedure for Polyphase Induction Motors and Generators (ANSI), IEEE Std 112-2004, 2004
[6] ***, Rotating Electrical Machines – Part 2-1: Standard Methods for Determining Losses and Efficiency from Tests (Excluding Machines for Traction Vehicles), IEC 60034-2-1:2014, 2014
[7] Alger, P. L., *Induction Machines – Their Behavior and Uses*, Gordon and Breach, 2nd ed., New York, USA, 1995
[8] Levi, E., *et al.*, Impact of Stray Load Losses on Vector Control Accuracy in Current-Fed Induction Motor Drives, *IEEE Transactions on Energy Conversion*, *1* (2006), 2, pp. 442-450
[9] Levi, E., *et al.*, Iron Loss in Rotor-Flux-Oriented Induction Machines: Identification, Assessment of Detuning, and Compensation, *IEEE Transactions on Power Electronics*, *11* (1996), 5, pp. 698-709
[10] Boglietti, A., *et al.*, Induction Motor Equivalent Circuit Including the Stray Load Losses in the Machine Power Balance, *IEEE Transactions on Energy Conversion*, *23* (2008), 3, pp. 796-803
[11] Shinnaka, S., Proposition of New Mathematical Models with Stator Core Loss Factor for Induction Motor, *Electrical Engineering in Japan*, *134* (2001), 1, pp. 64-75
[12] Bašić, M., *et al.*, Dynamic and Pole-Zero Analysis of Self-Excited Induction Generator Using a Novel Model with Iron Losses, *International Journal of Electrical Power & Energy Systems*, *42* (2012), 1, pp. 105-118
[13] Hasegawa, M., *et al.*, Vector Control of Induction Motors Using Full-Order Observer in Consideration of Core Loss, *IEEE Transactions on Industrial Electronics*, *50* (2003), 5, pp. 912-919
[14] Vamvakari, A., *et al.*, Analysis of Supply Voltage Distortion Effects on Induction Motor Operation, *IEEE Transactions on Energy Conversion*, *16* (2001), 3, pp. 209-213
[15] Chang, S. S. L., Physical Concepts or Stray Load Loss in Induction Machines, *Transactions of the American Institute of Electrical Engineers*, *73* (1954), 1, pp. 10-12
[16] Bašić, M., *et al.*, Wind Turbine-Driven Self-Excited Induction Generator: A Novel Dynamic Model Including Stray Load and Iron Losses, *Proceedings*, 2nd International Multidisciplinary Conference on Computer and Energy Science, SpliTech 2017, Split, Croatia, 2017
[17] ***, Rotating Electrical Machines – Part 30-1: Efficiency Classes of Line Operated AC Motors, IEC 60034-30-1, 2014
[18] Heier, S., *Grid Integration of Wind Energy Conversion Systems*, John Wiley & Sons Ltd, New York, USA, 1998
[19] Zaragoza, J., *et al.*, Study and Experimental Verification of Control Tuning Strategies in a Variable Speed Wind Energy Conversion System, *Renewable Energy*, *36* (2011), 5, pp. 1421-1430
[20] Martinez, F., *et al.*, Open Loop Wind Turbine Emulator, *Renewable Energy*, *63* (2014), Mar., pp. 212-221